The numerical study and solution verification of unsteady cavitation of a three-dimensional NACA hydrofoil with tubercles

Nicolaos Charalambous*, and Ian Eames*

*University College London (UCL) nicolaos.charalambous.13@ucl.ac.uk

1 Introduction

Cavitation is a prominent challenge in the field of hydromachinery and hydrofoil design, as it results in reduced propulsion efficiency and potential damage near surfaces. Extensive research has been conducted, encompassing both experimental and numerical investigations, to explore the correlation between hydrofoil flow and cavitation formation in flows around hydrofoils. The control of cavitation represents an area of ongoing research, which can be categorized into active control measures, involving the mitigation of cavitation through techniques such as water or bubble injection, and passive control measures, entailing modifications to the geometric characteristics of a hydrofoil or the utilization of different materials Xuemei et al. (2023), increase the roughness of the hydrofoil Asnaghi et al. (2020). In this study the interaction between a geometrical modified hydrofoil with tubercles and the effect on the cavitation dynamics using a computational method is presented. These hydrofoils were first studied by Fish et al. (1995) and were found to maintain an increase in the lift coefficient since the tubercles were delaying the stall. During the past few years, numerous researchers (Johari et al. (2015), Pendar et al. (2020)) have conducted experimental and computational studies to investigate the effects of tubercles on the enhanced performance of hydrofoils in the post-stall region.

In this study, the computational analysis focuses on investigating the flow characteristics around a NACA 0021 hydrofoil with tubercles of varying amplitude. To simulate the interaction between water and the vapour cloud, an Eulerian Volume of Fluid (VOF) solver is utilized. This solver tracks the interface by solving the continuity equation for the volume fraction of a single phase and incorporates a mass transfer rate fraction for the vapour, denoted as α_{ν} . The Schnerr-Sauer cavitation model is employed to calculate the mass transfer rate.

To account for turbulence, a Reynolds-Averaged Navier-Stokes (RANS) model is applied, specifically the k- ω SST turbulence model. Although for higher angles of attack it is recommended to use a turbulence that can capture

2 Geometry

In this study, three different geometries were investigated: two with tubercles and one without, as presented in Figure 1. The two configurations with tubercles were studied and presented, while the hydrofoil without tubercles served as the baseline reference. The profile of the hydrofoils used was the NACA0021. The hydrofoils with tubercles were defined by a sinusoidal geometry with an amplitude A and a wavelength λ . The values chosen for the amplitude and wavelength were the same as described by Custodio et al. (2017) and are shown in Table 1.

Table 1: Geometry of the hydrofoils

Hydrofoil	chord (mm)	span (mm)	A/c	λ/c
Baseline	102	102	-	-
8S	102	102	0.025	0.5
8L	102	102	0.12	0.5

3 Mesh and boundary conditions

In Figure 2, the boundary conditions and the computational domain used in the study are presented. The computational domain extends three times the chord length from the inlet boundary and seven times the

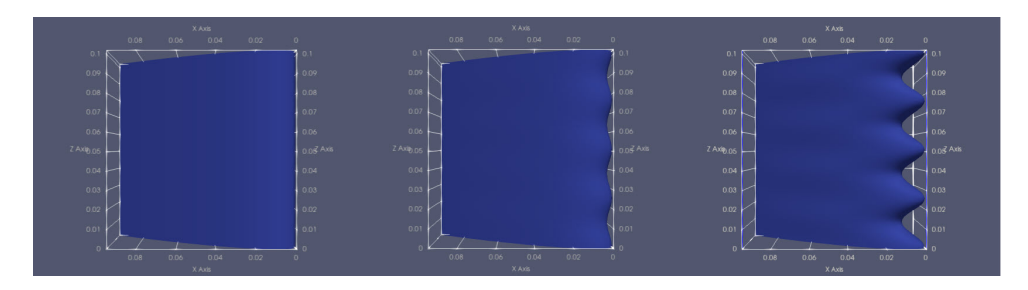


Fig. 1: Hydrofoils with tubercles an without used in the study

chord length to the outlet in the streamwise direction. The upper and bottom boundaries were extended 1.5 times the chord length in the vertical direction, and the spanwise boundaries were set to fit the span dimension of the hydrofoil. The cavitation number was set as a constant, $\sigma = 1$. The inflow velocity was set to U = 7.06 m/s with the pressure outlet p = 27100 Pa. The pressure was adjusted accordingly to ensure that the cavitation number always remained constant during the simulation. For the upper and lower walls, a no-slip condition was chosen, and for the side boundaries, a zero-gradient condition was applied.

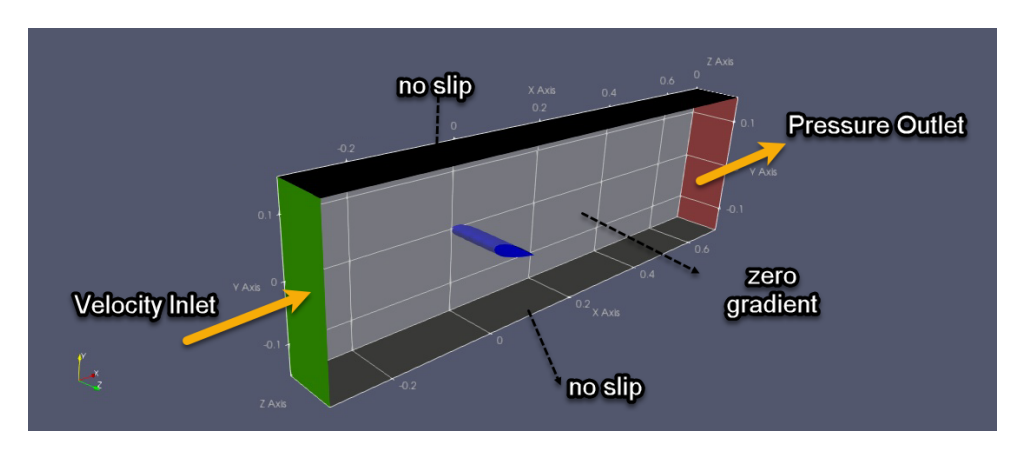


Fig. 2: Computational domain

The fluid properties chosen for the simulations are presented in table 2. The Courant number was set to 1 and the solver calculated the corresponding time step for the unsteady simulation, which ranged from 10^{-5} to 10^{-6} .

Fluid properties				
water density (kg/m^3)	997			
vapour density (kg/m^3)	0.02308			
water kinematic viscosity (m^2/s)	10^{-6}			
vapour kinematic viscosity (m^2/s)	$1.11 \cdot 10^{-3}$			
vapour pressure (Pa)	2300			
Reynolds number	$7.2 \cdot 10^{5}$			

Table 2: Fluids properties

The mesh was created using the blockMesh functionality in OpenFOAM, which allows the generation of structured grids, specifically hexahedral (hex) meshes. These meshes improve numerical accuracy and provide better capturing of the flow physics in multiphase flows. Moreover, these types of meshes are computationally efficient, requiring fewer cells, resulting in faster simulations and reduced memory

In Figure 3, the generated mesh is presented for a hydrofoil with tubercles at an angle of attack

of 22^{o} . A mesh sensitivity analysis was performed using the numerical solution verification method proposed by Negrato et al. (2017. Three different mesh resolutions were used, and the results for the lift and drag coefficients were compared. The numerical verification results for the lift and drag coefficients are shown in Table 3, where the different mesh sizes and corresponding coefficient values are presented. The y^+ for all meshes used were above 30 which is acceptable for the k- ω SST turbulence model that was used with the first cell located within the logarithmic layer , where the turbulence is developed and the wall function can provide a good prediction of the boundary layer

Table 3: Mesh resolutions used for the numerical verification for angle of attack $\alpha = 15^{\circ}$

Mesh ID	h_i/h_1	Mesh size (million)	C_L	C_D
Mesh 1	2.1	1.36	0.7389	0.085
Mesh 2	1.26	3.75	0.7452	0.098
Mesh 3	1.0	6.0	0.7612	0.109

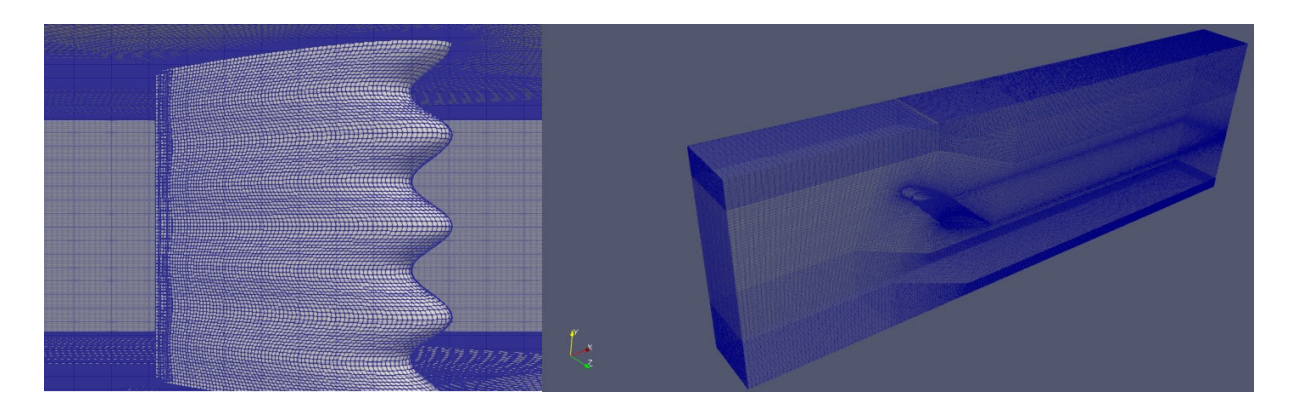


Fig. 3: Mesh around the NACA0021 hydrofoil

4 Methodology

An Eulerian method was applied to calculate the mixture of water and vapour by solving the continuity equation for the volume fraction of the vapour. The mass transfer rate due to cavitation used the Schnerr and Sauer cavitation model. Using the Eulerian method, the interphase between water and vapour can be resolved. To investigate potential areas of cavitation inception, a Lagrangian particle tracking method was employed to track the interference of particles with the cavitation cloud. The position of the particles and their speed can determine areas of nuclei concentration that can be a source of cavitation that cannot be modeled using the VOF method. The region close to the trailing edge where cavitation is detached from the hydrofoil surface and the flow is separated as well as the region were the re-entrant jet is visible are areas that could formulate the right conditions for the appearance of new nuclei that can lead to cavitation.

5 Results

In this section, we present the results for hydrofoils with and without tubercles, and we provide a comparison of their performance with respect to cavitation. Figure 4 illustrates the lift coefficient and drag coefficient for the three hydrofoils experiencing cavitation. On the x-axis, we include the nondimensional time \tilde{t} , calculated as follows:

$$\tilde{t} = \frac{\mathbf{U_{in}} * time}{c} \tag{1}$$

In this context U_{in} represents the inlet velocity, c denotes the chord length of the hydrofoils, and time signifies the simulation duration. The choice of the simulation time was made to ensure the completion of at least four cavitation cycles. In particular, when comparing the lift and drag coefficients for the

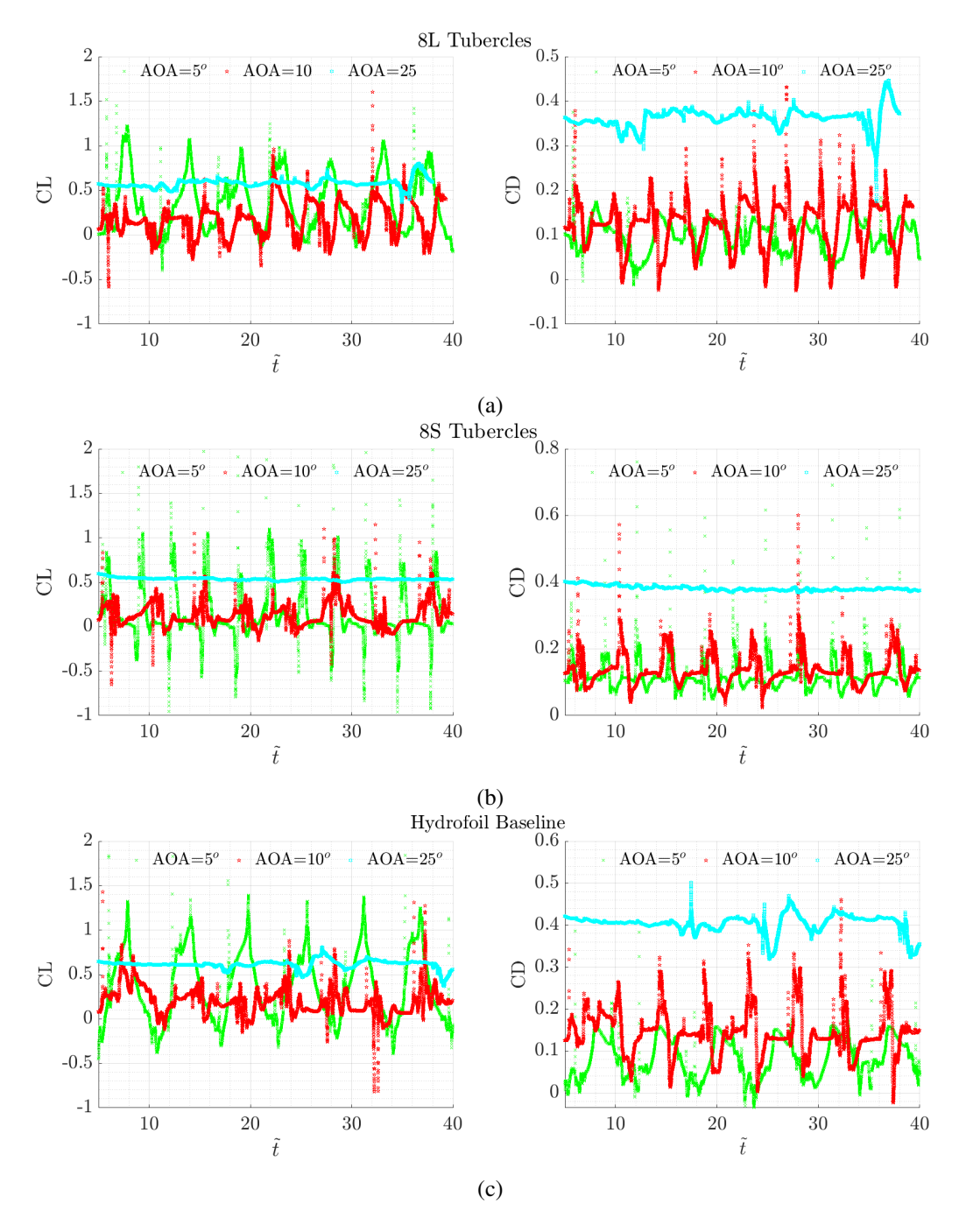


Fig. 4: Force Coefficients CL and CD (a) 8S Tubercles (b) 8L Tubercles (c) Baseline Hydrofoil

three hydrofoils, different fluctuation frequencies for the angle of attack were observed. The baseline hydrofoil exhibited higher lift at angles up to 15^{o} , but beyond to generate higher lift for angles up to 15^{o} angles of attack, but beyond 22 degrees, the lift coefficient experienced a sudden drop compared to hydrofoils with tubercles. The influence of tubercles became evident, particularly for large amplitudes, resulting in an increased average lift-to-drag ratio 7.33% at an angle of attack $AOA = 10^{o}$ and 18.84% for the $AOA = 25^{o}$ with regards to the lift to drag coefficient ratio. The Baseline hydrofoil had a higher value by 36% for AOA = 5. The pressure coefficients, as illustrated in 5, vary for different angles of attack and under different cavitation conditions, such as full sheet cavitation coverage or the onset of cavitation break-off. When sheet cavitation fully envelopes the hydrofoil, the pressure difference between the suction and pressure surfaces diminishes, and the pressure coefficient distribution between hydrofoils with tubercles and the baseline remains largely similar. Notably, distinctions in pressure distribution emerge when cavitation begins to break off. In such cases, the unsteadiness of the pressure distribution contributes to temporary peaks in lift until pressure stabilization occurs.

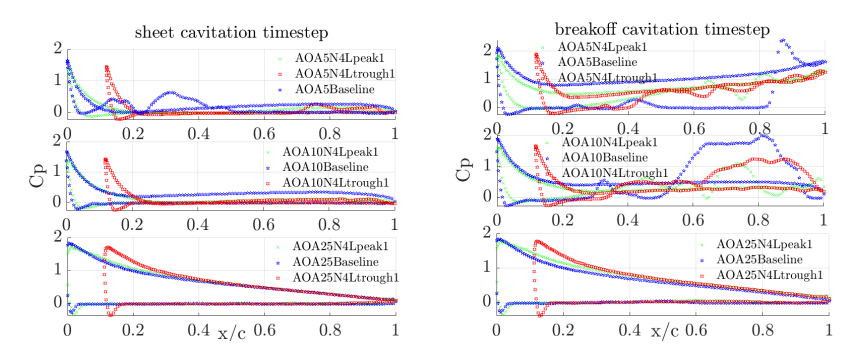


Fig. 5: Pressure coefficient for different angles of attack

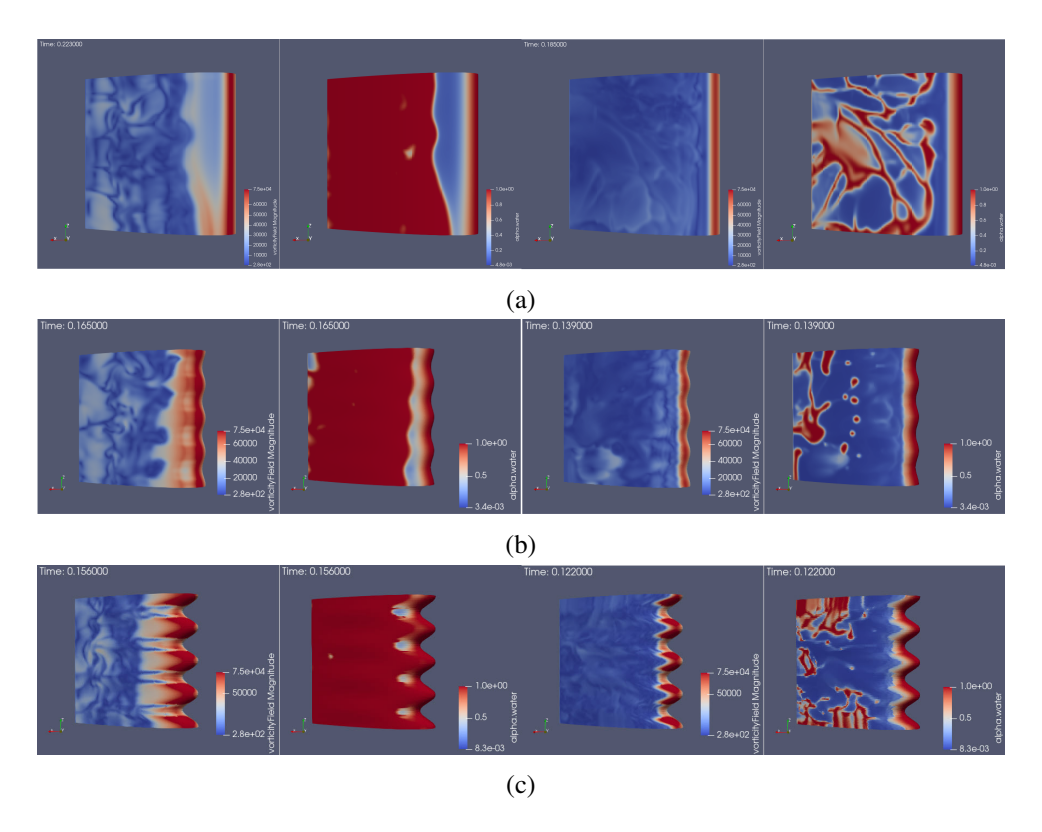


Fig. 6: The vorticity and vapor fraction were calculated at an angle of attack AOA=10° at two locations: at the end of the re-entrant jet and at the onset of sheet cavitation formation for: (a) Baseline hydrofoil (b) 8S hydrofoil with Tubercles (c) 8L hydrofoil with Tubercles

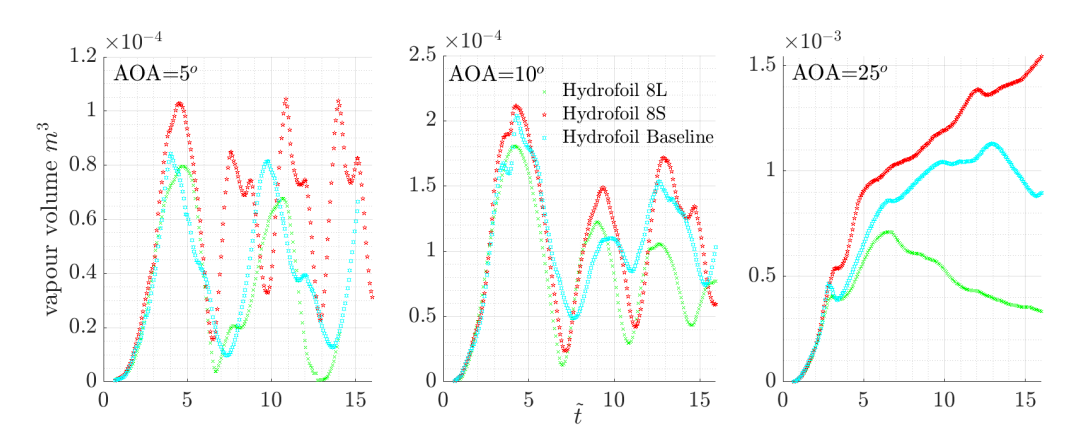


Fig. 7: The total vapour volume during the cavitation cycles

The generated vorticity plays a crucial role, as demonstrated in Figure 6, in cases involving fully cavitated hydrofoils and when initiating a new cavitation cycle. Hydrofoils with tubercles can influence both the vorticity morphology and the distribution of cavitation. Hydrofoils with higher amplitude tubercles appear to reduce vapor volume for specific angles of attack, as shown in Figure 7. Conversely, hydrofoils with smaller amplitude tubercles tend to increase cavitation volume, suggesting that tubercles can also serve as incipient cavitation inducers. The average reduction in cavitation volume can reach up to 19.8% for an angle of attack of $AOA=10^{\circ}$. This reduction may further increase with higher angles of attack.

6 Conclusions

In this study, we investigated hydrofoils both with and without tubercles for cavitation using a CFD method. The hydrofoils with tubercles exhibited a distinct cavitation cycle compared to those without tubercles. While the hydrofoils with tubercles showed a slightly smaller lift coefficient, at high angles of attack, the lift did not drop suddenly, as observed with the Baseline hydrofoils. In some instances, the lift-to-drag ratio for the hydrofoils with increased amplitude tubercles was higher.

The morphology of the detached cavitation cloud appeared to differ for the hydrofoils with tubercles, and the total volume of cavitation was calculated to be smaller. This study is ongoing, and we plan to include an assessment of the noise contribution of hydrofoils with tubercles in our future work."

References

Li Deyou, Y. Qi, Y. Weiqi, C. Hong and W. Hongjie (2021). Bionic leading-edge protuberances and hydrofoil cavitation. *Physics of Fluids*, **33**(9).

P. W. Weber, L. E. Howle, M. M. Murray, and D. S. Dally (2016). Computational evaluation of the performance of lifting surfaces with leading-edge protuberances. *J. Aircraft*, **48**(591 -600).

Li Xuemei, D. Jinxiong, Y. Weiqi, and S. Tiezhi (2021). How hydrofoil leading-edge biomimetic structure affects unsteady cavitating flow: A numerical study. *Physics of Fluids*, **35**(1).

A. Abolfazl, and R. Bensow (2020). Impact of Leading Edge Roughness in Cavitation. Fluids MDPI.

F. E. Fish, and J. M. Battle (1995). Hydrodynamic design of the humpback whale flipper. J. Morphol, 225(51-60).

P. Watts, and P. Fish (2001). The influence of passive, leading edge tubercles on wing performance. *In Proceedings of the 12th International Symposium on Unmanned Untethered Submersible Technology*.

C. Negrato, T. Lloyd, T.V. Terwisga, G. Vaz and R. Bensow (2017). Numerical Study of cavitation on NACA0015 Hydrofoil: Solution Verification. *MARINE* 2017.

H. Johari (2015). Cavitation on hydrofoils with sinusoidal leading edge. Journal of Physics, 656(1).

D. Custodio, C. Henoch and H. Johari (2018). Cavitation on hydrofoils with leading edge protuberances. *Ocean Engineering*, **162**(196-208).

M. R. Pendar, E. Esmaeilifar, E. Roohi (2020). LES study of unsteady cavitation characteristics of a 3-D hydrofoil with wavy leading edge. *Int. J. Multiphase Flow*, **132**(8).